Radiative transfer model: matrix operator method

Quanhua Liu and Eberhard Ruprecht

A radiative transfer model, the matrix operator method, is discussed here. The matrix operator method is applied to a plane–parallel atmosphere within three spectral ranges: the visible, the infrared, and the microwave. For a homogeneous layer with spherical scattering, the radiative transfer equation can be solved analytically. The vertically inhomogeneous atmosphere can be subdivided into a set of homogeneous layers. The solution of the radiative transfer equation for the vertically inhomogeneous atmosphere is obtained recurrently from the analytical solutions for the subdivided layers. As an example for the application of the matrix operator method, the effects of the cirrus and the stratocumulus clouds on the net radiation at the surface and at the top of the atmosphere are investigated. The relationship between the polarization in the microwave range and the rain rates is also studied. Copies of the FORTRAN program and the documentation of the FORTRAN program on a diskette are available.

Key words: Radiative transfer model, weighting function, clouds, rain.

1. Introduction

The matrix operator method (MOM) is one of the most commonly used methods for solving radiative transfer problems. The general model structure of the MOM can be taken from the literature.[1,2] Waterman[3] has presented an elegant matrix-exponential description for radiative transfer. He has derived analytical solutions for the transmission and reflection matrices in the limiting cases of $\delta \ll 1$ and $\delta \gg 1$, where δ is the optical depth. Our contribution to the MOM consists of analytical matrices for the transmission, reflection, and source function. The use of the analytical matrices in the derivation simplifies the MOM and reduces the computation time. The computation time does not increase with an increase of the scattering coefficient and the optical depth. An additional advantage of using the analytical matrices is that the weighting function for cloudy atmospheres and for various surface types can be directly obtained. We describe the MOM with our extension in Section 2. The theoretical description is written for both the shortwave and the longwave radiation. The microwave radiation transfer model is similar to the model for the other two spectral ranges, and it is described briefly. The gas absorption coefficients in the visible spectrum are taken from Kerschgens *et al.*[4] The gas absorption coefficients for the longwave radiation are taken from Schmetz.[5] The absorption coefficients in the microwave spectrum are adopted from Liebe.[6] The delta-M approximation for the phase function[7] in the visible and in the infrared ranges is applied to reduce the number of required Fourier expansion terms. Various surface types[8,9] are also included in the code.

2. Matrix Operator Method

The radiative transfer model described here is applicable to a plane–parallel medium. Spherical particles for aerosols and clouds are assumed. The model is used into two versions: a nonpolarized version for shortwave and longwave radiation, and a polarized version for microwave radiation.

A. Shortwave and Longwave Radiation

The equation describing the monochromatic radiative transfer through a plane–parallel medium

E. Ruprecht is with the Institut für Meereskunde, University of Kiel, Düsternbrooker weg 20, D24105 Kiel, Germany. Q. Liu is with the Alfred Wegener Institute for Polar and Marine Research, Am Handelshafen 12, D-27570 Bremerhaven, Germany.

Received 21 August 1995; revised manuscript received 29 January 1996.

0003-6935/96/214229-09$10.00/0

reads[10]

$$-\mu \frac{dL(\tau, \mu, \phi; \mu_0, \phi_0)}{d\tau} = L(\tau, \mu, \phi; \mu_0, \phi_0) - (1 - \varpi)B(T) - \frac{\varpi}{2\pi} \times P(\mu, \phi; \mu_0, \phi_0)S_0 \exp(-\tau/\mu_0) - \frac{\varpi}{2\pi} \times \int_0^{2\pi} \int_{-1}^{1} P(\mu, \phi; \mu', \phi')L(\tau, \mu', \phi'; \mu_0, \phi_0) \times d\mu' d\phi', \quad (1)$$

where $\mu_0 \geq 0$ is the cosine of the Sun zenith angle, ϕ_0 is the Sun azimuth angle, S_0 is the solar spectral constant, ϖ is the single-scattering albedo, $B(T)$ is Planck's function for temperature T, P is the phase function, and L is the intensity of the diffuse radiation with $\mu \geq 0$ and $\mu < 0$ for the downward and upward directions, respectively. By introducing the total intensity (radiance)

$$I(\tau, \mu, \phi; \mu_0, \phi_0) = L(\tau, \mu, \phi; \mu_0, \phi_0) + S_0 \exp(-\tau/\mu_0)\delta(\mu - \mu_0)\delta(\phi - \phi_0), \quad (2)$$

We can rewrite Eq. (1) as

$$-\mu \frac{dI(\tau, \mu, \phi; \mu_0, \phi_0)}{d\tau} = I(\tau, \mu, \phi; \mu_0, \phi_0) - (1 - \varpi)B(T) - \frac{\varpi}{2\pi} \times \int_0^{2\pi} \int_{-1}^{1} P(\mu, \phi; \mu', \phi')I(\tau, \mu', \phi'; \mu_0, \phi_0) \times d\mu' d\phi', \quad (3)$$

with the boundary conditions

$$I(0, \mu, \phi; \mu_0, \phi_0) = S_0\delta(\mu - \mu_0)\delta(\phi - \phi_0) \quad \text{for } \mu \geq 0 \quad (4a)$$

at the top, and

$$I(\tau_s, \mu, \phi; \mu_0, \phi_0) = \epsilon(\mu)B(T) + \int_0^{2\pi} \int_0^{1} r(\mu, \phi; \mu', \phi') \times I(\tau_s, \mu', \phi'; \mu_0, \phi_0)\mu' d\mu' d\phi', \quad (4b)$$

$$\epsilon(\mu) + \int_0^{2\pi} \int_0^{1} r(\mu, \phi; \mu', \phi')\mu' d\mu' d\phi' = 1 \quad (4c)$$

at the surface. Here r is the surface reflectance and $\delta(x - x_0)$ is the delta function.

Equation (3) can be solved in a matrix form (i.e., with the MOM) through the Fourier expansion for the azimuth angle and discretizing zenith angles. With the Fourier expansion the following approximations are obtained for the radiance and for the phase function, respectively:

$$I(\mu, \phi; \mu_0, \phi_0) = \sum_{m=0}^{N} I_m(\mu, \mu_0)\cos m(\phi - \phi_0), \quad (5a)$$

$$P(\mu, \phi; \mu', \phi') = \sum_{m=0}^{N} P_m(\mu, \mu')\cos m(\phi - \phi'). \quad (5b)$$

Inserting Eqs. (5) into Eq. (3), we have the radiative transfer equation for each Fourier component:

$$-\mu \frac{dI_m(\tau, \mu, \mu_0)}{d\tau} = I_m(\tau, \mu, \mu_0) - \frac{\varpi}{2}(1 + \delta_{0m}) \int_{-1}^{1} P_m(\mu, \mu') \times I_m(\tau, \mu', \mu_0)d\mu' - (1 - \varpi)B(T)\delta_{0m}, \quad (6)$$

where $\delta_{ij} = 1$ for $i = j$, and $\delta_{ij} = 0$ for $i \neq j$.

With the introduction of a discrete method for the zenith angle, Eq. (6) can be rewritten in matrix form:

$$\frac{d}{d\tau}\begin{bmatrix} \mathbf{I}_m^+ \\ \mathbf{I}_m^- \end{bmatrix} = -\begin{bmatrix} \varpi\mathbf{M}^{-1}\mathbf{P}_m^+\mathbf{C} - \mathbf{M}^{-1} & \varpi\mathbf{M}^{-1}\mathbf{P}_m^-\mathbf{C} \\ -\varpi\mathbf{M}^{-1}\mathbf{P}_m^-\mathbf{C} & -\varpi\mathbf{M}^{-1}\mathbf{P}_m^+\mathbf{C} + \mathbf{M}^{-1} \end{bmatrix} \times \begin{bmatrix} \mathbf{I}_m^+ \\ \mathbf{I}_m^- \end{bmatrix} - (1 - \varpi)B(T)\delta_{0m}\begin{bmatrix} \mathbf{M}^{-1} \\ -\mathbf{M}^{-1} \end{bmatrix} = -\begin{bmatrix} \mathbf{A}_1^m & \mathbf{A}_2^m \\ -\mathbf{A}_2^m & -\mathbf{A}_1^m \end{bmatrix}\begin{bmatrix} \mathbf{I}_m^+ \\ \mathbf{I}_m^- \end{bmatrix} - (1 - \varpi)B(T)\delta_{0m}\begin{bmatrix} \mathbf{M}^{-1} \\ -\mathbf{M}^{-1} \end{bmatrix}. \quad (7)$$

In this equation $\mathbf{P}_m^+ = [P_m^+(\mu, \mu')]$ is the forward scattering matrix where both μ and μ' have the same sign, $\mathbf{P}_m^- = [P_m^-(\mu, \mu')]$ is the backward scattering matrix where both μ and μ' have the opposite sign, $\mathbf{M} = [\mu_i\delta_{ij}]$ is the diagonal matrix, $\mathbf{C} = [c_i\delta_{ij}]$ is the diagonal matrix with c_i as the integration weight, $\mathbf{A}_1^m = \omega\mathbf{M}^{-1}\mathbf{P}_m^+\mathbf{C} - \mathbf{M}^{-1}$, $\mathbf{A}_2^m = \omega\mathbf{M}^{-1}\mathbf{P}_m^-\mathbf{C}$, $\mathbf{I}_m^-$ is the downward radiance matrix, and $\mathbf{I}_m^+$ is the upward radiance matrix.

In the following paragraphs, the indices for wavelength and the Fourier component are omitted. The solution[11] of Eq. (7) for a homogeneous layer of an optical thickness δ is (see Fig. 1)

$$\begin{bmatrix} \mathbf{I}_0^+ \\ \mathbf{I}_\delta^- \end{bmatrix} = \begin{bmatrix} \mathbf{T} & \mathbf{R} \\ \mathbf{R} & \mathbf{T} \end{bmatrix}\begin{bmatrix} \mathbf{I}_\delta^+ \\ \mathbf{I}_0^- \end{bmatrix} + \begin{bmatrix} \mathbf{J}_\delta^+ \\ \mathbf{J}_\delta^- \end{bmatrix}, \quad (8)$$

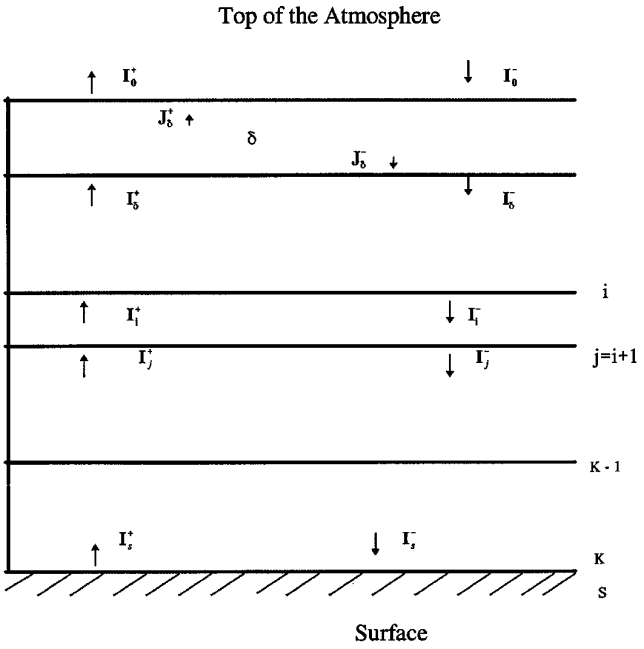

Fig. 1. Scheme of the layered atmosphere for the radiation transfer calculation.

where the transmission, reflection, and source matrices are

$$\mathbf{T} = 2[\cosh(\mathbf{H}\delta) - \mathbf{V}\ \sinh(\mathbf{H}\delta) + \cosh(\mathbf{F}\delta) - \mathbf{U}\ \sinh(\mathbf{F}\delta)]^{-1}, \tag{9a}$$

$$\mathbf{R} = \tfrac{1}{2}[\cosh(\mathbf{H}\delta) + \mathbf{V}\ \sinh(\mathbf{H}\delta) - \cosh(\mathbf{F}\delta) - \mathbf{U}\ \sinh(\mathbf{F}\delta)]\mathbf{T}, \tag{9b}$$

$$\mathbf{J}_\delta{}^+ = \mathbf{J}_\delta{}^- = (\mathbf{E} - \mathbf{T} - \mathbf{R})B(T)[\mathbf{1}] \tag{9c}$$

for the zeroth Fourier component, and $\mathbf{J}_\delta{}^+ = \mathbf{J}_\delta{}^- = [\mathbf{0}]$ for the nonzeroth Fourier components. Here $\mathbf{E}$ is the unit matrix, $[\mathbf{1}]$ is the matrix with all elements equal to one, $[\mathbf{0}]$ is the zero matrix in which all elements equal zero, and

$$\mathbf{H}^2 = (\mathbf{A}_1 - \mathbf{A}_2)(\mathbf{A}_1 + \mathbf{A}_2), \quad \mathbf{F}^2 = (\mathbf{A}_1 + \mathbf{A}_2)(\mathbf{A}_1 - \mathbf{A}_2), \tag{10a}$$

$$\mathbf{V} = (\mathbf{A}_1 + \mathbf{A}_2)\mathbf{H}^{-1}, \quad \mathbf{U} = (\mathbf{A}_1 - \mathbf{A}_2)F^{-1}. \tag{10b}$$

Equations (9) are the full solution of the radiative transfer model for one homogeneous layer. In order get the solution for any atmospheric profile, the vertically inhomogeneous atmosphere is subdivided into K homogeneous layers (Fig. 1). With this procedure the transmission, reflection, and source matrices for the vertically inhomogeneous atmosphere can be calculated from the transmission, reflection, and source matrices of the K homogeneous layers in recurrence. Then the solution of Eq. (3) at any level i can be obtained in recurrence[12]:

$$\begin{bmatrix}\mathbf{I}_i{}^+\\ \mathbf{I}_i{}^-\end{bmatrix} = \begin{bmatrix}(\mathbf{E} - \mathbf{R}_{ij}\mathbf{R}_{i0})^{-1}\mathbf{R}_{ij}\mathbf{T}_{0i} & (\mathbf{E} - \mathbf{R}_{ij}\mathbf{R}_{i0})^{-1}\mathbf{T}_{ji}\\ (\mathbf{E} - \mathbf{R}_{i0}\mathbf{R}_{ij})^{-1}\mathbf{T}_{0i} & (\mathbf{E} - \mathbf{R}_{i0}\mathbf{R}_{ij})^{-1}\mathbf{R}_{i0}\mathbf{T}_{ji}\end{bmatrix}\begin{bmatrix}\mathbf{I}_0{}^-\\ \mathbf{I}_j{}^+\end{bmatrix} + \begin{bmatrix}(\mathbf{E} - \mathbf{R}_{ij}\mathbf{R}_{i0})^{-1}(\mathbf{J}_{ji}{}^+ + \mathbf{R}_{ij}\mathbf{J}_{0i}{}^-)\\ \mathbf{R}_{i0}(\mathbf{E} - \mathbf{R}_{ij}\mathbf{R}_{i0})^{-1}\mathbf{J}_{ji}{}^+ + (\mathbf{E} - \mathbf{R}_{i0}\mathbf{R}_{ij})^{-1}\mathbf{J}_{0i}{}^-\end{bmatrix}, \tag{11}$$

where

$$\mathbf{R}_{j0} = \mathbf{R}_{ji} + \mathbf{T}_{ij}(\mathbf{E} - \mathbf{R}_{i0}\mathbf{R}_{ij})^{-1}\mathbf{R}_{i0}\mathbf{T}_{ji}, \tag{12a}$$

$$\mathbf{R}_{0j} = \mathbf{R}_{0i} + \mathbf{T}_{i0}(\mathbf{E} - \mathbf{R}_{ij}\mathbf{R}_{i0})^{-1}\mathbf{R}_{ij}\mathbf{T}_{0i}, \tag{12b}$$

$$\mathbf{T}_{j0} = \mathbf{T}_{i0}(\mathbf{E} - \mathbf{R}_{ij}\mathbf{R}_{i0})^{-1}\mathbf{T}_{ji}, \tag{12c}$$

$$\mathbf{T}_{0j} = \mathbf{T}_{ij}(\mathbf{E} - \mathbf{R}_{i0}\mathbf{R}_{ij})^{-1}\mathbf{T}_{0i}, \tag{12d}$$

$$\begin{bmatrix}\mathbf{J}_{j0}{}^+\\ \mathbf{J}_{0j}{}^-\end{bmatrix} = \begin{bmatrix}\mathbf{T}_{i0}(\mathbf{E} - \mathbf{R}_{ij}\mathbf{R}_{i0})^{-1} & \mathbf{0}\\ \mathbf{T}_{ij}(\mathbf{E} - \mathbf{R}_{i0}\mathbf{R}_{ij})^{-1}\mathbf{R}_{i0} & \mathbf{E}\end{bmatrix}\begin{bmatrix}\mathbf{J}_{ji}{}^+\\ \mathbf{J}_{ij}{}^-\end{bmatrix} + \begin{bmatrix}\mathbf{E} & \mathbf{T}_{i0}(\mathbf{E} - \mathbf{R}_{ij}\mathbf{R}_{i0})^{-1}\mathbf{R}_{ij}\\ 0 & \mathbf{T}_{ij}(\mathbf{E} - \mathbf{R}_{i0}\mathbf{R}_{ij})^{-1}\end{bmatrix} \times \begin{bmatrix}\mathbf{J}_{i0}{}^+\\ \mathbf{J}_{0i}{}^-\end{bmatrix}. \tag{12e}$$

It is worth pointing out that $\mathbf{R}_{j0} \neq \mathbf{R}_{0j}$ for an inhomogeneous layer, that is, the reflectance at the bottom differs from the reflectance at the top for the inhomogeneous layer.

B. Boundary Conditions

By the definition of the surface reflection matrix, $\mathbf{R}_g$, the radiance at the surface (index s) is

$$\mathbf{I}_s{}^- = \mathbf{R}_{s0}\mathbf{I}_s{}^+ + \mathbf{T}_{0s}\mathbf{I}_0{}^- + \mathbf{J}_{0s}{}^-, \tag{13a}$$

$$\mathbf{I}_s{}^+ = \mathbf{e}_g\mathbf{B}(\mathbf{T}_s) + \mathbf{R}_g\mathbf{I}_s{}^-, \tag{13b}$$

emissivity matrix $\mathbf{e}_g$ is

$$\mathbf{e}_g = \begin{bmatrix}\epsilon(\mu_1) & \epsilon(\mu_1) & \cdots & \epsilon(\mu_1)\\ \epsilon(\mu_2) & \epsilon(\mu_2) & \cdots & \epsilon(\mu_2)\\ \vdots & & \ddots & \vdots\\ \epsilon(\mu_n) & \epsilon(\mu_n) & \cdots & \epsilon(\mu_n)\end{bmatrix} \tag{14}$$

for the zeroth Fourier component and its elements are determined by Eq. (4c), and $\mathbf{e}_g = [\mathbf{0}]$ for the other Fourier components. From Eqs. (13) the boundary condition at the surface can be written as

$$\mathbf{I}_s{}^+ = \mathbf{e}_g\mathbf{B}(\mathbf{T}_s) + \mathbf{R}_g(\mathbf{E} - \mathbf{R}_{s0}\mathbf{R}_g)^{-1} \times [\mathbf{R}_{s0}\mathbf{e}_g\mathbf{B}(\mathbf{T}_s) + \mathbf{T}_{0s}\mathbf{I}_0{}^- + \mathbf{J}_{0s}{}^-]. \tag{15}$$

The boundary condition at the top of the atmosphere

is

$$\mathbf{I}_0^- = \frac{S_0}{2}\mathbf{C}^{-1}, \tag{16a}$$

$$\mathbf{I}_0^- = S_0\mathbf{C}^{-1} \tag{16b}$$

for the zeroth and nonzeroth Fourier components, respectively. The spectral solar constant is taken from Froehlich and Brusa,[13] and this constant has been adopted by the World Meteorological Organization. The dependence of spectral solar constant S_0 on time and latitude is also considered.[14] From Eqs. (12)–(16) we obtain a closed solution in the MOM for an Earth atmospheric system.

C. Microwave Radiation

The solution of the microwave radiative transfer equation is similar to the solution in the visible and the infrared spectra with the exception of the use of the Stokes vector $[I_v\ I_h\ U\ V]^t$ (t denoting a transpose) to replace the intensity and the use of the phase matrix to replace the phase function. For spherical particles, phase matrix $\mathbf{P}(\Theta)$ is[15]

$$\mathbf{P}(\Theta) = \begin{bmatrix} M_0 & 0 & 0 & 0 \\ 0 & M_1 & 0 & 0 \\ 0 & 0 & S_{21} & -D_{21} \\ 0 & 0 & D_{21} & S_{21} \end{bmatrix}. \tag{17}$$

The Rayleigh phrase matrix applies for particles of small size compared with the electromagnetic wavelength; it is given by

$$\mathbf{P}(\Theta) = \frac{3}{8\pi}\begin{bmatrix} \cos^2\Theta & 0 & 0 & 0 \\ 0 & 1 & 0 & 0 \\ 0 & 0 & \cos\Theta & 0 \\ 0 & 0 & 0 & \cos\Theta \end{bmatrix}. \tag{18}$$

Phase matrix $\mathbf{P}(\Theta)$ is defined in the scattering plane, which contains both the incident and outgoing directions. The Stokes vector is defined in a meridional plane containing the z axis and the outgoing direction. Therefore, phase matrix $\mathbf{P}(\Theta)$ has to be transferred by multiplication of the rotation matrices to the scattering phase matrix, $\mathbf{S}$, which is defined in the meridional plane. The rotation matrix is

$$\mathbf{L}(\varphi) = \begin{bmatrix} \cos^2\varphi & \sin^2\varphi & \tfrac{1}{2}\sin(2\varphi) & 0 \\ \sin^2\varphi & \cos^2\varphi & -\tfrac{1}{2}\sin(2\varphi) & 0 \\ -\sin(2\varphi) & \sin(2\varphi) & \cos(2\varphi) & 0 \\ 0 & 0 & 0 & 1 \end{bmatrix}. \tag{19}$$

Then the scattering matrix is defined by

$$\mathbf{S} = \mathbf{L}(\pi - i_2)\mathbf{P}(\Theta)\mathbf{L}(i_1), \tag{20}$$

where rotation angle i_1 is the angle between the incoming ray and the scattering plane, and i_2 is the angle between the outgoing ray and the scattering plane.

To simplify the formulation, we neglect the influence from the solar radiation on the microwave radiation. In this case the Stokes vector is independent of the azimuth angle, and the integration of element S_{ij} of scattering matrix $\mathbf{S}$ over azimuth angle ϕ becomes[16]

$$\int_0^{2\pi} S_{ij}\mathrm{d}\phi = 0 \tag{21}$$

for $ij = 13, 14, 23, 24, 31, 32, 41$, and 42.

Thus, the first two components of the Stokes vector are decoupled from the other two components of the Stokes vector. The microwave radiative transfer equation can then be written as

$$-\mu\frac{\mathrm{d}}{\mathrm{d}\tau}\begin{bmatrix} I_v \\ I_h \end{bmatrix} = \begin{bmatrix} I_v \\ I_h \end{bmatrix} - \varpi\int_{-1}^{1}\begin{bmatrix} P_{vv} & P_{vh} \\ P_{hv} & P_{hh} \end{bmatrix}\begin{bmatrix} I_v \\ I_h \end{bmatrix}\mathrm{d}\mu - (1-\varpi)\begin{bmatrix} B(T) \\ B(T) \end{bmatrix}, \tag{22}$$

where

$$P_{vv} = \int_0^{2\pi} S_{11}\mathrm{d}\phi, \quad P_{vh} = \int_0^{2\pi} S_{12}\mathrm{d}\phi,$$

$$P_{hh} = \int_0^{2\pi} S_{22}\mathrm{d}\phi, \quad P_{hv} = \int_0^{2\pi} S_{21}\mathrm{d}\phi,$$

with the extension

$$\mathbf{I}^+ = \begin{bmatrix} \mathbf{I}_v^+ \\ \mathbf{I}_h^+ \end{bmatrix}, \quad \mathbf{I}^- = \begin{bmatrix} \mathbf{I}_v^- \\ \mathbf{I}_h^- \end{bmatrix},$$

$$\mathbf{A}_1 = \omega\begin{bmatrix} \mathbf{M}^{-1} & 0 \\ 0 & \mathbf{M}^{-1} \end{bmatrix}\mathbf{P}^+\begin{bmatrix} \mathbf{C} & \mathbf{0} \\ \mathbf{0} & \mathbf{C} \end{bmatrix} - \begin{bmatrix} \mathbf{M}^{-1} & \mathbf{0} \\ \mathbf{0} & \mathbf{M}^{-1} \end{bmatrix},$$

$$\mathbf{A}_2 = \omega\begin{bmatrix} \mathbf{M}^{-1} & \mathbf{0} \\ \mathbf{0} & \mathbf{M}^{-1} \end{bmatrix}\mathbf{P}^-\begin{bmatrix} \mathbf{C} & \mathbf{0} \\ \mathbf{0} & \mathbf{C} \end{bmatrix},$$

$$\mathbf{P}^+ = \begin{bmatrix} P_{vv}^+(\mu, \mu') & P_{vh}^+(\mu, \mu') \\ P_{hv}^+(\mu, \mu') & P_{hh}^+(\mu, \mu') \end{bmatrix},$$

$$\mathbf{P}^- = \begin{bmatrix} P_{vv}^-(\mu, \mu') & P_{vh}^-(\mu, \mu') \\ P_{hv}^-(\mu, \mu') & P_{hh}^-(\mu, \mu') \end{bmatrix}.$$

Equations (12)–(16) provide a full solution to the microwave radiative transfer equation. In the microwave range, Planck function $B(T)$ is usually replaced by the brightness temperature through the Rayleigh–Jean approximation.

D. Delta-*M* Approximation

A large number of terms of the Legendre polynomial expansions are required to treat the strongly asym-

metric phase function of aerosols and clouds in the visible spectrum. Therefore, we apply the delta-M approximation for the phase function in the visible and the infrared spectra. Eight moments of the Mie phase function are used in our calculations, which can "guarantee 4–6 significant digits in fluxes" (see Ref. 7). The delta-M approximation is not applied in the microwave range because the phase function in the microwave range is smooth.

E. Surface Reflectance

For the different spectral ranges, surface emissivity and reflectance have to be handled in different ways. For the infrared radiation, the surface emissivity is set to a constant (e.g., $\epsilon = 1$). For the shortwave radiation, vegetated land, water surface with different surface winds, and a Lambert surface of the different surface reflectance are used. The Lambert surface and the water surface are also used in the microwave radiative transfer model.

For a Lambert surface the reflected radiation field is isotropic. In this case the surface reflection factor with a surface albedo ω_g is given by

$$r_g = \frac{\omega_g}{\pi}. \tag{23a}$$

The surface reflection matrix can then be calculated as

$$\mathbf{R}_g = 2\omega_g[\mathbf{1}]\mathbf{MC} \tag{23b}$$

for the zeroth Fourier component [definition of $\mathbf{M}$ and $\mathbf{C}$, see below Eq. (7)], and

$$\mathbf{R}_g = [\mathbf{0}] \tag{23c}$$

for the nonzeroth Fourier components.

Surfaces with reflection factors departing from ω_g/π are called anisotropic surfaces. Nearly all surfaces have a strong anisotropic behavior at large viewing zenith angles and large Sun zenith angles. The reflection factors over vegetated lands are taken from Kriebel.[8] For water surfaces the roughness induced by sea surface wind should be considered. The surface bidirectional reflectance factor of water surfaces in the visible range is defined by

$$R(\theta, \phi; \theta_0, \phi_0) = \frac{r(\Theta)\exp(-\tan^2\theta_n/\sigma^2)}{4\sigma^2 \cos\theta \cos\theta_0 \cos^4\theta_n}, \tag{24}$$

where $\cos 2\Theta = \cos\theta\cos\theta_0 + \sin\theta\sin\theta_0\cos(\phi - \phi_0)$, $\cos\theta_n = (\cos\theta + \cos\theta_0)/(2\cos\Theta)$, $r(\Theta) = \frac{1}{2}[|R_v(\Theta)|^2 + |R_h(\Theta)|^2]$, with the local Fresnel coefficients

$$R_h(\Theta) = \frac{\cos\Theta - (\epsilon - \sin^2\Theta)^{1/2}}{\cos\Theta + (\epsilon - \sin^2\Theta)^{1/2}}, \tag{25a}$$

$$R_v(\Theta) = \frac{\epsilon\cos\Theta - (\epsilon - \sin^2\Theta)^{1/2}}{\epsilon\cos\Theta + (\epsilon - \sin^2\Theta)^{1/2}}, \tag{25b}$$

in which ϵ is the complex relative dielectric constant.

Slope variance σ^2 is calculated after Cox and Munk,[17]

$$\sigma^2 = 0.003 + 0.00512V, \tag{26}$$

with wind V (m/s) at 10 m above the sea surface. The coverage of the sea surface with foam is calculated from the formulation of Stogryn[18]:

$$f = 7.751 \times 10^{-6} V^{3.231}. \tag{27}$$

The effective reflectance of foam is 22% according to Koepke.[19] The total bidirectional reflectance factor is then

$$R(\theta, \phi; \theta_0, \phi_1) = (1 - f)\frac{r(\Theta)\exp(-\tan^2\theta_n/\sigma^2)}{4\sigma^2 \cos\theta \cos\theta_0 \cos^4\theta_n} + 0.22f. \tag{28}$$

The surface reflectance within the microwave radiation range should also be extended to the Stokes reflection matrix. For calm water, spectral reflection matrix r is defined by

$$r(\Theta) = \begin{bmatrix} |R_v|^2 & 0 & 0 & 0 \\ 0 & |R_h|^2 & 0 & 0 \\ 0 & 0 & \mathrm{Re}(R_v R_h^*) & -\mathrm{Im}(R_v R_h^*) \\ 0 & 0 & \mathrm{Im}(R_v R^*) & \mathrm{Re}(R_v R_h^*) \end{bmatrix}. \tag{29}$$

An empirical formulation of the sea surface reflectance with sea surface wind V is taken from Wisler and Hollinger.[20] The vertically polarized reflectance, Γ_v, is

$$\Gamma_v = f\left[1 - \frac{208 + 1.29v}{T_s}(1 - 9.946 \times 10^{-4}\theta + 3.218 \times 10^{-5}\theta^2 - 1.187 \times 10^{-6}\theta^3 + 7 \times 10^{-20}\theta^{10})\right] + (1 - f)\left\{|R_v|^2 - \frac{V[0.117 - 2.09 \times 10^{-3}\exp(7.32 \times 10^{-2}\theta)]\sqrt{v}}{T_s}\right\}, \tag{30a}$$

and the horizontally polarized reflectance, Γ_h, is

$$\Gamma_h = f\left[1 - \frac{208 + 1.29v}{T_s}(1 - 1.748 \times 10^{-3}\theta - 7.336 \times 10^{-5}\theta^2 + 1.044 \times 10^{-7}\theta^3)\right] + (1 - f) \times \left[|R_h|^2 - \frac{V(0.115 + 3.8 \times 10^{-5}\theta^2)\sqrt{v}}{T_s}\right], \tag{30b}$$

where T_s is the sea surface temperature in degrees Kelvin, v is the frequency in gigahertz, θ is the incident angle in degrees, and f is the foam coverage given by Eq. (27).

3. Results

In order to show the performance and accuracy of our method, a comparison of the transmission and reflection is carried out with the present method and with the double-adding method[2] for a homogeneous cloudy layer and for Sun zenith angles of 0° and 84.14°. The Henyey–Greenstein phase function with an asymmetry factor $g = 0.8$ and a single-scattering albedo $\varpi = 0.8$ are used. Results from both methods agree in six digits for optical thicknesses between zero and 64 (Tables 1 and 2). The applicability of our method is demonstrated with three examples: weighting function, effect of clouds on the radiation budget, and the relationship between the polarization (i.e., $TB_v - TB_h$) and rain rates.

A. Weighting Function

The weighting function used in remote sensing gives the contribution of the atmospheric layer to the satellite measurements. It is an important factor for the design of radiometers and retrieval algorithms. The weighting function for the clear-sky atmosphere is well discussed.[21] The general expression of the weighting function (with clouds) can be derived from the matrix operator method (see Appendix A). It can be seen from Eq. (A8) in Appendix A that the weighting function for any homogeneous layer ij is composed of the upwelling radiation from layer ij and the surface reflected downwelling radiation from layer ij. The upwelling source function contributed by layer ij at the top of the atmosphere is composed of two components [see Eq. (A3)]: the radiation emitted from the top of layer ij and the radiation emitted from the bottom of layer ij. The contribution of layer ij to the downwelling source function at the surface is calculated in a similar way [see Eq. (A2)]. The weighting functions for 37 GHz at a viewing angle of 50° are calculated for a U.S. Standard Atmosphere profile with and without clouds over a water surface. The cloud top is at 4 km, and within the cloud a homogeneous rain rate of 5 mm/h is assumed. For the clear-sky case the maximum of the weighting functions is found at the ground (0.3 for horizontal polarization, 0.55 for vertical polarization; see Fig. 2). At ~500 m above ground the weighting functions fall off to 0.05 and decrease further with height. The larger values of the weighting functions for the vertical polarization at the surface are due to the larger surface emissivity in the vertical polarization.

Opposite results are found in the atmospheric layer, because the surface reflected downwelling radiation [see Eq. (A8)] from the atmospheric layer is

Table 1. Comparison of the Transmission Calculated with the Present and the Double-Adding Methods for $\varpi = 0.8$ and the Henyey–Greenstein Phase Function[a]

	Sun Zenith Angle (deg)			
	0		84.14	
δ	Double Adding	Present	Double Adding	Present
0.00	1.00000000	1.00000000	1.00000000	1.00000000
0.10	0.97588945	0.97588945	0.66704434	0.66704434
0.25	0.93958977	0.93958977	0.44304325	0.44304324
0.50	0.87959291	0.87959291	0.30406781	0.30406780
1.00	0.76348895	0.76348895	0.20309545	0.20309544
2.00	0.56268617	0.56268617	0.11542966	0.11542966
3.00	0.40405572	0.40405590	0.07182829	0.07182834
4.00	0.28511198	0.28511175	0.04632729	0.04632724
8.00	0.06424282	0.06424283	0.00901064	0.00901064
16.00	0.00282852	0.00282851	0.00038015	0.00038015
32.00	0.00000519	0.00000519	0.00000070	0.00000070
64.00	0.00000000	0.00000000	0.00000000	0.00000000

[a]Asymmetry factor $g = 0.8$; optical thickness δ varies from 0 to 64.

Table 2. Comparison of the Reflection Calculated with the Present and the Double-Adding Methods for $\varpi = 0.8$ and the Henyey–Greenstein Phase Function[a]

	Sun Zenith Angle (deg)			
	0		84.14	
δ	Double Adding	Present	Double Adding	Present
0.00	0.00000000	0.00000000	0.00000000	0.00000000
0.10	0.00389969	0.00389969	0.17716067	0.17716067
0.25	0.00932527	0.00932527	0.27329390	0.27329391
0.50	0.01735193	0.01735193	0.31790959	0.31790960
1.00	0.03037980	0.03037980	0.33888981	0.33888981
2.00	0.04679583	0.04679583	0.34945320	0.34945321
3.00	0.05538106	0.05538128	0.35239008	0.35239010
4.00	0.05968337	0.05968337	0.35344672	0.35344678
8.00	0.06348576	0.06348572	0.35415805	0.35415807
16.00	0.06367621	0.06367621	0.35418554	0.35418562
32.00	0.06367657	0.06367657	0.35418558	0.35418575
64.00	0.06367657	0.06367658	0.35418558	0.35418592

[a]Asymmetry factor $g = 0.8$; optical thickness δ varies from 0 to 64.

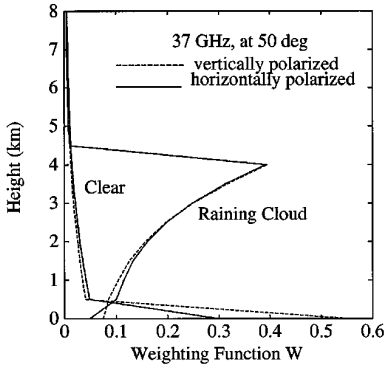

Fig. 2. Weighting function for 37 GHz at a viewing angle of 50° for clear and cloudy atmospheres. The raining cloud is assumed to be a homogeneous cloud with a rain rate of 5 mm/h. The cloud top is at 4 km above water surface.

larger in the horizontal polarization. For the cloudy case the maximum contribution to signal at the top of the atmosphere comes from the cloud top layer (0.4), with a drastic decrease above (less than 0.05) and a slight decrease below (~0.1 just above the surface). The two weighting functions for horizontally and vertically polarized radiation are almost identical; only in the lowest 1.5 km above ground do small differences occur. The explanation of these differences is the same as for the clear-sky case. The very small differences near the cloud top are due to the effect of the residual polarization in the cloud.

B. Effects of Clouds on Net Radiation

Another field of application is the cloud–radiation interaction. We apply the method to different clouds over a desert and over a water surface. The atmospheric states are described by a tropical atmospherical profile for the first case and by a U.S. Standard Atmosphere profile for latter. Cirrus clouds with a top at 12 km and low stratocumulus clouds with a top at 3 km are assumed. Both cloud types are 1 km thick with varying optical thickness at 0.55 μm (0–10 for cirrus, 0–30 for stratocumulus).[22] The solar zenith angle is set to 60° and the length of the day is 12 h. Figure 3 shows the large radiation loss, F, which is not compensated by absorption Q. Thus the net radiation flux at the top of the atmosphere over a bright desert is always negative ($Q < F$); this result was observed in the Earth Radiation Budget Experiment.[23] The reason is well known; the desert has a high surface albedo, which reflects a large part of solar radiation back to space; the remaining radiation is almost totally used to increase the surface temperature, which leads to high thermal emission. Over a water surface the situation is in general opposite to the case over a desert, at least for cirrus clouds (Fig. 4). The absorbed solar radiation increases (by almost a factor of 2) because of the small albedo of the water, and the outgoing longwave radiation is slightly decreased. Only for thick stratocumulus clouds is the net radiation negative ($F > Q$). For very thick clouds (optical thickness greater than 20), the surface becomes more and more unimportant for the radiation budget at the top of the atmosphere.

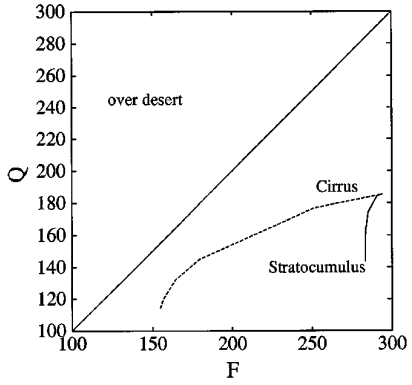

Fig. 3. Absorbed solar radiation and outgoing longwave radiation (Q and F, respectively, in watts times inverse square meters) at the top of the atmosphere. A tropical atmospherical profile over desert is used. The cloud is 1 km thick and its top is at 12 km for cirrus and at 3 km for stratocumulus clouds. The optical thickness at 0.55 μm is between 0 and 10 for the cirrus and between 0 and 30 for the stratocumulus.

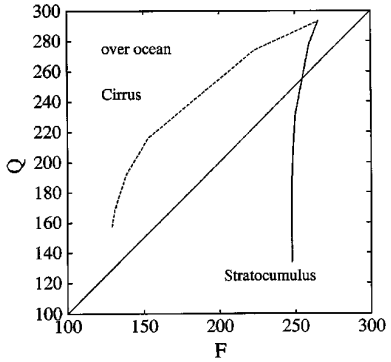

Fig. 4. Same as Fig. 3, but for clouds over a water surface and for a U.S. Standard Atmosphere profile.

The radiation budget at the surface is always positive in cloud-free situations, and it is usually positive even in cloudy situations (Figs. 5 and 6). Only for thick cirrus clouds (optical thickness greater than 6) over the desert is the budget negative ($F > Q$), because the absorbed solar radiation, Q, is reduced by clouds whereas the net longwave radiation remains almost constant. This means that most of the contribution of the downwelling radiation comes from the atmospheric column beneath the cirrus cloud base. The large amount of the longwave downwelling radiation over the desert can be estimated by comparing Figs. 5 and 6. The net longwave radiation is much smaller at the desert surface than over the ocean, despite the warmer land surface. The two figures also demonstrate that a cloud with an optical thickness of 30 is not yet in the saturation phase for short-wave radiation, whereas for long-

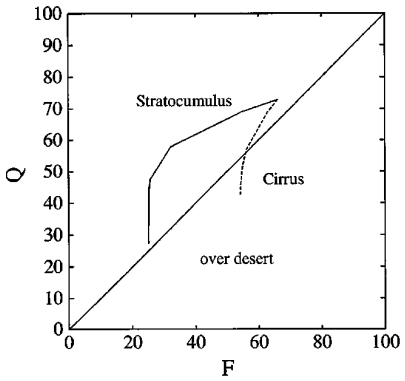

Fig. 5. Net solar radiation and net longwave radiation (Q and F, respectively, as in Fig. 3) at the surface. A tropical atmospheric profile over a desert is used. The cloud is 1 km thick and its top is at 12 km for cirrus and at 3 km for stratocumulus clouds. The optical thickness at 0.55 μm is between 0 and 10 for the cirrus and between 0 and 30 for the stratocumulus.

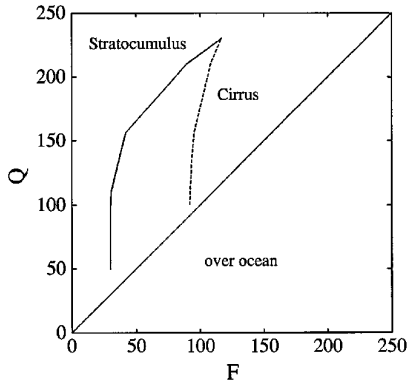

Fig. 6. Same as Fig. 5, but for clouds over a water surface and for a U.S. Standard Atmosphere profile.

wave radiation F barely changes when the optical thickness for cirrus clouds is above 6 and for stratocumulus clouds above 10.

C. Polarization and Rain Rates

As an example for the application of our method in the microwave spectral range, we calculated the brightness temperatures for two polarization states and for the frequencies of 6.6, 19.35, and 37 GHz. A homogeneous raining cloud is assumed with a cloud top at a height of 4 km. The rain rates from 0 to 50 mm/h are constant with height. In Fig. 7 the relationship is shown between polarization differences in logarithm scale and rain rates. An almost linear decrease exists for 6.6 GHz over the total range of the rain rates, in contrast to the other two frequencies, which reach saturation very soon at ~25 mm/h for 19.35 GHz and at 7 mm/h for 37 GHz. The advantage of the sensitivity at the latter two frequencies is counteracted by the saturation. We also have to consider the poorer spatial resolution at lower frequencies when a decision is to be made concerning which frequencies should be used for the rainfall retrieval.

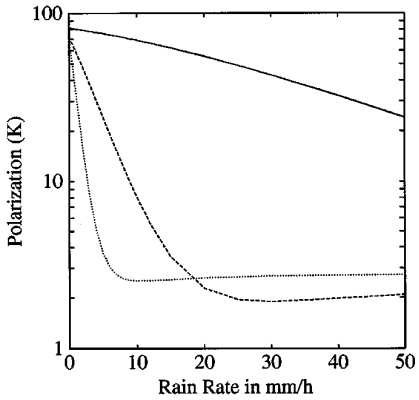

Fig. 7. Variation of the polarization difference $(TB_v - TB_h)$ at 53° with rain rates. A U.S. Standard Atmosphere profile over a sea surface is used. The cloud top is at 4 km above the sea surface and the rain rate is homogeneous from the sea surface to the cloud top. The solid, dashed, and dotted curves are for 6.6, 19.35, and 37 GHz, respectively.

4. Conclusion

The matrix operator method described here is applied to a plane-parallel atmosphere in the visible, infrared, and microwave ranges. The use of analytical matrices for the transmission, reflection, and source function in the MOM reduces the computation time, and the computation time also does not increase with the increase of the scattering coefficient and the optical depth.

An additional advantage is that the weighting function for cloudy atmospheres and for various surface types within the infrared and microwave ranges can be analytically obtained in the matrix form. From examples shown in Section 3 we can conclude that the method is a very helpful and efficient tool that can be applied to different problems in radiation transfer.

Appendix A.

For the total atmospheric layer from the top to the bottom of the atmosphere, the source function in Eq. (12e) can be written as

$$\begin{aligned}
\begin{bmatrix}\mathbf{J}_{s0}^{+}\\ \mathbf{J}_{0s}^{-}\end{bmatrix} &= \begin{bmatrix}\mathbf{T}_{j0}(\mathbf{E}-\mathbf{R}_{js}\mathbf{R}_{j0})^{-1} & \mathbf{0}\\ \mathbf{T}_{js}(\mathbf{E}-\mathbf{R}_{j0}\mathbf{R}_{js})^{-1}\mathbf{R}_{j0} & \mathbf{E}\end{bmatrix}\begin{bmatrix}\mathbf{J}_{sj}^{+}\\ \mathbf{J}_{js}^{-}\end{bmatrix}\\
&\quad+\begin{bmatrix}\mathbf{E} & \mathbf{T}_{j0}(\mathbf{E}-\mathbf{R}_{js}\mathbf{R}_{j0})^{-1}\mathbf{R}_{js}\\ \mathbf{0} & \mathbf{T}_{js}(\mathbf{E}-\mathbf{R}_{j0}\mathbf{R}_{js})^{-1}\end{bmatrix}\begin{bmatrix}\mathbf{J}_{j0}^{+}\\ \mathbf{J}_{0j}^{-}\end{bmatrix}\\
&= \begin{bmatrix}\mathbf{T}_{j0}(\mathbf{E}-\mathbf{R}_{js}\mathbf{R}_{j0})^{-1} & \mathbf{0}\\ \mathbf{T}_{js}(\mathbf{E}-\mathbf{R}_{j0}\mathbf{R}_{js})^{-1}\mathbf{R}_{j0} & \mathbf{E}\end{bmatrix}\begin{bmatrix}\mathbf{J}_{sj}^{+}\\ \mathbf{J}_{js}^{-}\end{bmatrix}\\
&\quad+\begin{bmatrix}\mathbf{E} & \mathbf{T}_{j0}(\mathbf{E}-\mathbf{R}_{js}\mathbf{R}_{j0})^{-1}\mathbf{R}_{js}\\ \mathbf{0} & \mathbf{T}_{js}(\mathbf{E}-\mathbf{R}_{j0}\mathbf{R}_{js})^{-1}\end{bmatrix}\\
&\quad\times\begin{bmatrix}\mathbf{T}_{i0}(\mathbf{E}-\mathbf{R}_{ij}\mathbf{R}_{i0})^{-1} & \mathbf{0}\\ \mathbf{T}_{ij}(\mathbf{E}-\mathbf{R}_{i0}\mathbf{R}_{ij})^{-1}\mathbf{R}_{i0} & \mathbf{E}\end{bmatrix}\begin{bmatrix}\mathbf{J}_{ji}^{+}\\ \mathbf{J}_{ij}^{-}\end{bmatrix}\\
&\quad+\begin{bmatrix}\mathbf{E} & \mathbf{T}_{j0}(\mathbf{E}-\mathbf{R}_{js}\mathbf{R}_{j0})^{-1}\mathbf{R}_{js}\\ \mathbf{0} & \mathbf{T}_{js}(\mathbf{E}-\mathbf{R}_{j0}\mathbf{R}_{js})^{-1}\end{bmatrix}\\
&\quad\times\begin{bmatrix}\mathbf{E} & \mathbf{T}_{ij}(\mathbf{E}-\mathbf{R}_{ij}\mathbf{R}_{i0})^{-1}\mathbf{R}_{ij}\\ \mathbf{0} & \mathbf{T}_{ij}(\mathbf{E}-\mathbf{R}_{i0}\mathbf{R}_{ij})^{-1}\end{bmatrix}\begin{bmatrix}\mathbf{J}_{i0}^{+}\\ \mathbf{J}_{0i}^{-}\end{bmatrix}, \qquad \text{(A1)}
\end{aligned}$$

where layer ij is any homogeneous layer (see Fig. 1). The contribution of layer ij to the upwelling source function at the top and the downwelling source function at the bottom is determined by the second term on the right-hand side of Eq. (A1). Thus, the contribution of layer ij to the downwelling source function $\mathbf{J}_{0s}^{-}$ can be obtained from Eq. (A1):

$$\begin{aligned}
\mathbf{C}_i^d &= \mathbf{B}_i^d B(\overline{T}_i)\\
&= \mathbf{T}_{js}(\mathbf{E}-\mathbf{R}_{j0}\mathbf{R}_{js})^{-1}(\mathbf{E}-\mathbf{T}_{ij}-\mathbf{R}_{ij})B(\overline{T}_i)\\
&\quad+\mathbf{T}_{js}(\mathbf{E}-\mathbf{R}_{j0}\mathbf{R}_{js})^{-1}\mathbf{T}_{ij}(\mathbf{E}-\mathbf{R}_{i0}\mathbf{R}_{ij})^{-1}\\
&\quad\times\mathbf{R}_{i0}(\mathbf{E}-\mathbf{T}_{ij}-\mathbf{R}_{ij})B(\overline{T}_i). \qquad \text{(A2)}
\end{aligned}$$

The contribution of layer ij to the upwelling source function $\mathbf{J}_{s0}^{+}$ can be written as

$$\begin{aligned}\mathbf{C}_i^{u} &= \mathbf{B}_i^{u} B(\overline{T}_i) \\ &= \mathbf{T}_{i0}(\mathbf{E} - \mathbf{R}_{is}\mathbf{R}_{i0})^{-1}(\mathbf{E} - \mathbf{T}_{ij} - \mathbf{R}_{ij})B(\overline{T}_i) \\ &\quad + \mathbf{T}_{i0}(\mathbf{E} - \mathbf{R}_{is}\mathbf{R}_{i0})^{-1}\mathbf{T}_{ij}(\mathbf{E} - \mathbf{R}_{js}\mathbf{R}_{ij})^{-1} \\ &\quad \times \mathbf{R}_{js}(\mathbf{E} - \mathbf{T}_{ij} - \mathbf{R}_{ij})B(\overline{T}_i), \end{aligned} \tag{A3}$$

where $\overline{T}_i$ is the mean temperature of layer ij, and the source function for layer ij is given by

$$\begin{aligned}\mathbf{J}_{ji}^{+} &= \mathbf{J}_{ij}^{-} \\ &= (\mathbf{E} - \mathbf{T}_{ij} - \mathbf{R}_{ij})B(\overline{T}_i). \end{aligned} \tag{A4}$$

To derive Eq. (A3) from Eq. (A1) we use the following relationship:

$$\begin{aligned}&\mathbf{T}_{i0}(\mathbf{E} - \mathbf{R}_{is}\mathbf{R}_{i0})^{-1} + \mathbf{T}_{i0}(\mathbf{E} - \mathbf{R}_{is}\mathbf{R}_{i0})^{-1}\mathbf{T}_{ij}(\mathbf{E} - \mathbf{R}_{is}\mathbf{R}_{ij})^{-1} \\ &\quad \times \mathbf{R}_{js} = \mathbf{T}_{i0}(\mathbf{E} - \mathbf{R}_{ij}\mathbf{R}_{i0})^{-1} + \mathbf{T}_{j0}(\mathbf{E} - \mathbf{R}_{js}\mathbf{R}_{j0})^{-1} \\ &\quad \times \mathbf{R}_{js}(\mathbf{E} + \mathbf{T}_{ij}(\mathbf{E} - \mathbf{R}_{i0}\mathbf{R}_{ij})^{-1}\mathbf{R}_{i0}. \end{aligned} \tag{A5}$$

The upwelling infrared and microwave radiation at the top of the atmosphere can be expressed by

$$\begin{aligned}\mathbf{I}_0^{+} &= \mathbf{T}_{s0}\mathbf{I}_s^{+}[\mathbf{1}] + \mathbf{J}_{s0}^{+}[\mathbf{1}] \\ &= \mathbf{T}_{s0}(\mathbf{E} - \mathbf{R}_g\mathbf{R}_{s0})^{-1}\mathbf{e}_g[\mathbf{1}]B(T_s) \\ &\quad + \mathbf{T}_{s0}(\mathbf{E} - \mathbf{R}_g\mathbf{R}_{s0})^{-1}\mathbf{R}_g\mathbf{J}_{0s}^{-}[\mathbf{1}] + \mathbf{J}_{s0}^{+}[\mathbf{1}] \\ &= \mathbf{W}_K B(T_s) + \sum_{i=0}^{K-1} \mathbf{W}_i B(T_i)\Delta h_i, \end{aligned} \tag{A6}$$

where the weighting functions are given by

$$\mathbf{W}_K = \mathbf{T}_{s0}(\mathbf{E} - \mathbf{R}_g\mathbf{R}_{s0})^{-1}\mathbf{e}_g[\mathbf{1}], \tag{A7}$$

$$\begin{aligned}\mathbf{W}_i &= \frac{1}{\Delta h_i}\mathbf{B}_i^{u}[\mathbf{1}] + \frac{1}{\Delta h_i}\mathbf{T}_{s0}(\mathbf{E} - \mathbf{R}_g\mathbf{R}_{s0})^{-1}\mathbf{R}_g\mathbf{B}_i^{d}[\mathbf{1}] \\ &= [\mathbf{T}_{i0}(\mathbf{E} - \mathbf{R}_{is}\mathbf{R}_{i0})^{-1} + \mathbf{T}_{i0}(\mathbf{E} - \mathbf{R}_{is}\mathbf{R}_{i0})^{-1} \\ &\quad \times \mathbf{T}_{ij}(\mathbf{E} - \mathbf{R}_{js}\mathbf{R}_{ij})^{-1}\mathbf{R}_{js} + \mathbf{T}_{s0}(\mathbf{E} - \mathbf{R}_g\mathbf{R}_{s0})^{-1} \\ &\quad \times \mathbf{R}_g[\mathbf{T}_{js}(\mathbf{E} - \mathbf{R}_{j0}\mathbf{R}_{js})^{-1} + \mathbf{T}_{js}(\mathbf{E} - \mathbf{R}_{j0}\mathbf{R}_{js})^{-1} \\ &\quad \times \mathbf{T}_{ij}(\mathbf{E} - \mathbf{R}_{i0}\mathbf{R}_{ij})^{-1}\mathbf{R}_0]](\mathbf{E} - \mathbf{T}_{ij} - \mathbf{R}_{ij})[\mathbf{1}]\frac{1}{\Delta h_i}, \end{aligned} \tag{A8}$$

where $\Delta h_i = z_i - z_j$, and z is the height at level i. Matrices $\mathbf{T}_{i0}$, $\mathbf{T}_{js}$, $\mathbf{T}_{s0}$, $\mathbf{T}_{ij}$, $\mathbf{R}_{is}$, $\mathbf{R}_{i0}$, $\mathbf{R}_{js}$, $\mathbf{R}_{ij}$, $\mathbf{R}_{s0}$, and $\mathbf{R}_{j0}$ in Eq. (A8) can be calculated from Eqs. (9a) and (9b) and Eqs. (12a)–(12d).

References

1. G. N. Plass, G. W. Kattawar, and F. E. Catchings, "Matrix operator theory of radiative transfer. 1. Rayleigh scattering," Appl. Opt. **12,** 314–329 (1973).
2. J. Fischer and H. Grassl, "Radiative transfer in an atmosphere-ocean system: an azimuthally dependent matrix operator approach," Appl. Opt. **23,** 1032–1039 (1984).
3. P. C. Waterman, "Matrix-exponential description of radiative transfer," J. Opt. Soc. Am. **71,** 410–422 (1981).
4. M. Kerschgens, E. Raschke, and U. Reuter, "The absorption of solar radiation in model atmospheres," Contrib. Atmos. Phys. **49,** 81–97 (1976).
5. J. Schmetz, "An atmospheric-correction scheme for operational application to METEOSAT infrared measurements," ESA J. **10,** 145–159 (1986).
6. H. J. Liebe, "An updated model for millimeter wave propagation in moist air," Radio Sci. **20,** 1069–1089 (1985).
7. W. J. Wiscombe, "The Delta-m method: rapid yet accurate radiative flux calculations for strongly asymmetric phase function," J. Atmos. Sci. **34,** 1408–1422 (1977).
8. K. T. Kriebel, "Measured spectral bidirectional reflection properties of four vegetated surfaces," Appl. Opt. **17,** 253–259 (1978).
9. E. D. Bowker and R. E. Davis, "Spectral reflectances of natural targets for use in remote sensing studies," NASA Ref. Publ. **1139,** 1–184 (1985).
10. S. Chandrasekhar, *Radiative Transfer* (Dover, New York, 1960).
11. Q. Liu, C. Simmer, and E. Ruprecht, "A general analytical expression of the radiation source function for emitting and scattering media within the matrix operator method," Contrib. Atmos. Phys. **64,** 73–82 (1991).
12. Q. Liu, "A radiative budget index at the top of the atmosphere derived from METEOSAT climate data set," Report of Institut für Meereskunde, University of Kiel, Nr 216 1991).
13. C. Froehlich and R. W. Brusa, "Solar radiation and its variation," Sol. Phys. **74,** 209–215 (1981).
14. M. Iqbal, *An Introduction to Solar Radiation* (Academic, New York, 1983).
15. H. C. Van de Hulst, *Light Scattering by Small Particles* (Wiley, New York, 1957).
16. L. Tsang, J. A. Kong, and R. T. Shin, *Theory of Microwave Remote Sensing* (Wiley-Interscience, New York, 1985).
17. C. Cox and W. Munk, "Measurement of the roughness of the sea surface from photography of the Sun's glitter," J. Opt. Soc. Am. **44,** 828–850 (1954).
18. A. Stogryn, "The emissivity of sea foam at microwave frequencies," J. Geophys. Res. **77,** 1658–1666 (1972).
19. P. Koepke, "The reflectance factors of a rough ocean with foam—comment on 'Remote sensing of the sea state using the 0.8–1.1 μm spectral band' by L. Wald and J. M. Monget," Int. J. Remote Sensing **6,** 787–799 (1985).
20. M. M. Wisler and J. P. Hollinger, "Estimation of marine environmental parameters using microwave radiometric remote sensing systems," NRL Memo. 3661 (Naval Research Laboratories, Washington, D.C., 1977).
21. S. Q. Kidder and T. H. Vonder Haar, *Satellite Meteorology* (Academic, New York, 1995).
22. J. E. Hansen, "Multiple scattering of polarized light in planetary atmospheres. Part II: sunlight reflected by terrestrial water clouds," J. Atmos. Sci. **28,** 1400–1426 (1971).
23. E. Raschke, T. H. Vonder Haar, W. R. Bandeen, and M. Pasternak, "The annual radiation balance of the earth-atmosphere system during 1969–1970 from Nimbus-3 measurements," J. Atmos. Sci. **30,** 341–364 (1973).